Size dependent stability of cobalt nanoparticles on silica under high conversion Fischer-Tropsch environment

Moritz Wolf, Hendrik Kotzé, Nico Fischer and Michael Claeys*

Supplementary information

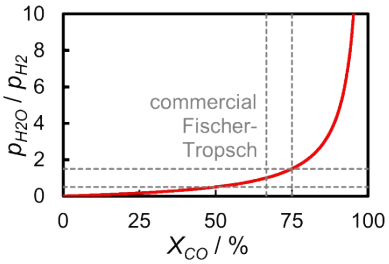

Fig. S1 Theoretical calculation of the partial pressure ratio of H_2O to H_2 as a function of CO conversion (*red*, *solid*) in the Fischer-Tropsch synthesis assuming a feed gas composition and stoichiometric consumption of H_2 to CO of 2. The data is superimposed on typical operation conditions of the cobalt based low temperature Fischer-Tropsch synthesis.

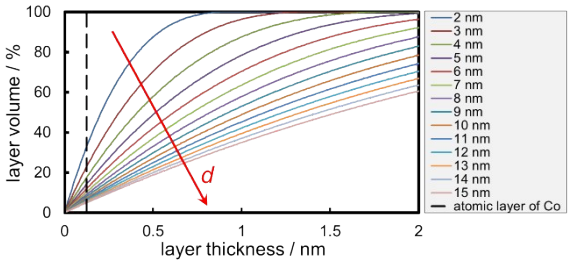

Fig. S2 Theoretical calculation of the volume of an outer layer relative to the volume of the whole sphere as a function of layer thickness for several diameters.

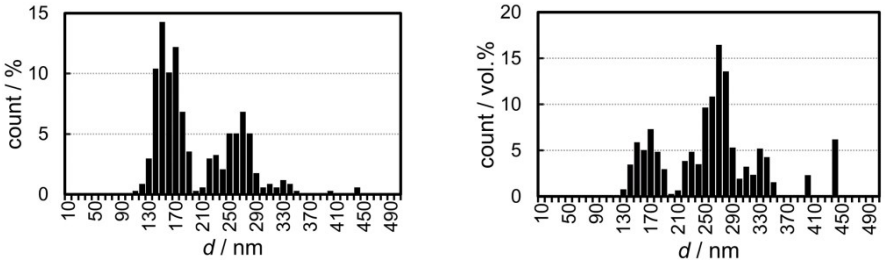

Fig. S3 Number based (*left*) and volume based (*right*) size distribution of the Stöber silica spheres as obtained via TEM.

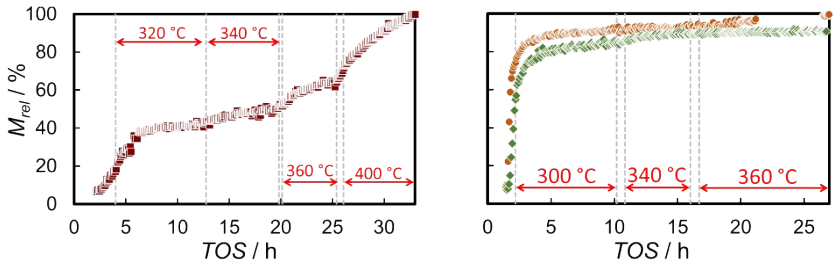

Fig. S4 Magnetisation at maximal field strength relative to the magnetisation after reduction of CAT A (*red squares*; *left*), CAT B (*orange circles*), and CAT C (*green diamonds*; *right*) as a function of time on stream at several reduction temperatures.

*Catalysis Institute and c*change (DST-NRF Centre of Excellence in Catalysis), Department of Chemical Engineering, University of Cape Town, Private Bag X3, Rondebosch 7701, South Africa. E-mail: michael.claeys@uct.ac.za*

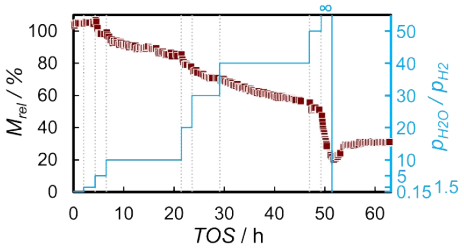

Fig. S5 Magnetisation at maximal field strength relative to the magnetisation after reduction of CAT A (*red squares*) as a function of the original time on stream with stepwise increase of the ratio of partial pressures of H_2O to H_2 (*blue, solid*).

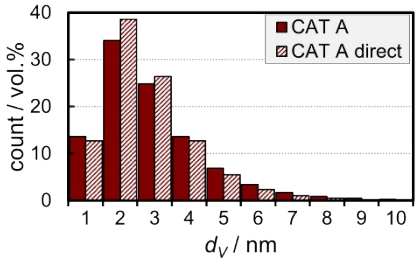

Fig. S6 Size distributions of the metallic cobalt crystallites in CAT A after exposure to H_2O level 1-7 (*filled bars*) and direct exposure of freshly reduced CAT A to H_2O level 7 (*patterned bars*) obtained via the application of the Langevin equation.

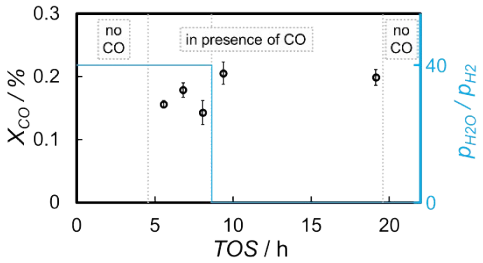

Fig. S7 Absolute conversion of CO on CAT A (*black circles*) as a function of time on with a high initial ratio of partial pressures of H_2O to H_2 (*blue, solid*).

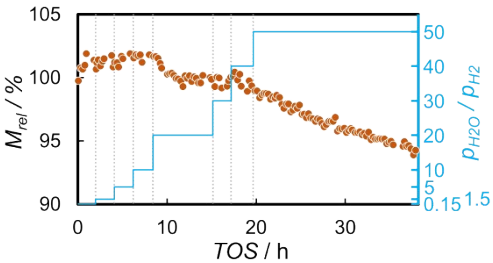

Fig. S8 Magnetisation at maximal field strength relative to the magnetisation after reduction of CAT B in absence of CO (*orange circles*) as a function of the original time on stream with stepwise increase of the ratio of partial pressures of H_2O to H_2 (*blue, solid*).

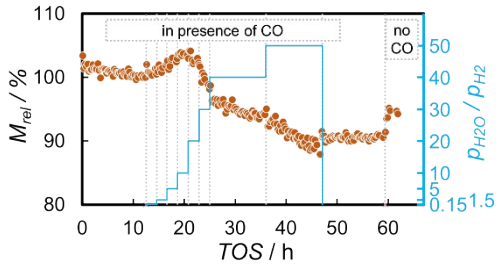

Fig. S9 Magnetisation at maximal field strength relative to the magnetisation after reduction of CAT B in presence of CO (*orange circles*) as a function of the original time on stream with stepwise increase of the ratio of partial pressures of H_2O to H_2 (*blue, solid*).

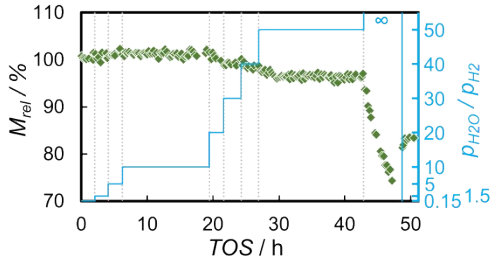

Fig. S10 Magnetisation at maximal field strength relative to the magnetisation after reduction of CAT C (*green diamonds*) as a function of the original time on stream with stepwise increase of the ratio of partial pressures of H_2O to H_2 (*blue, solid*).

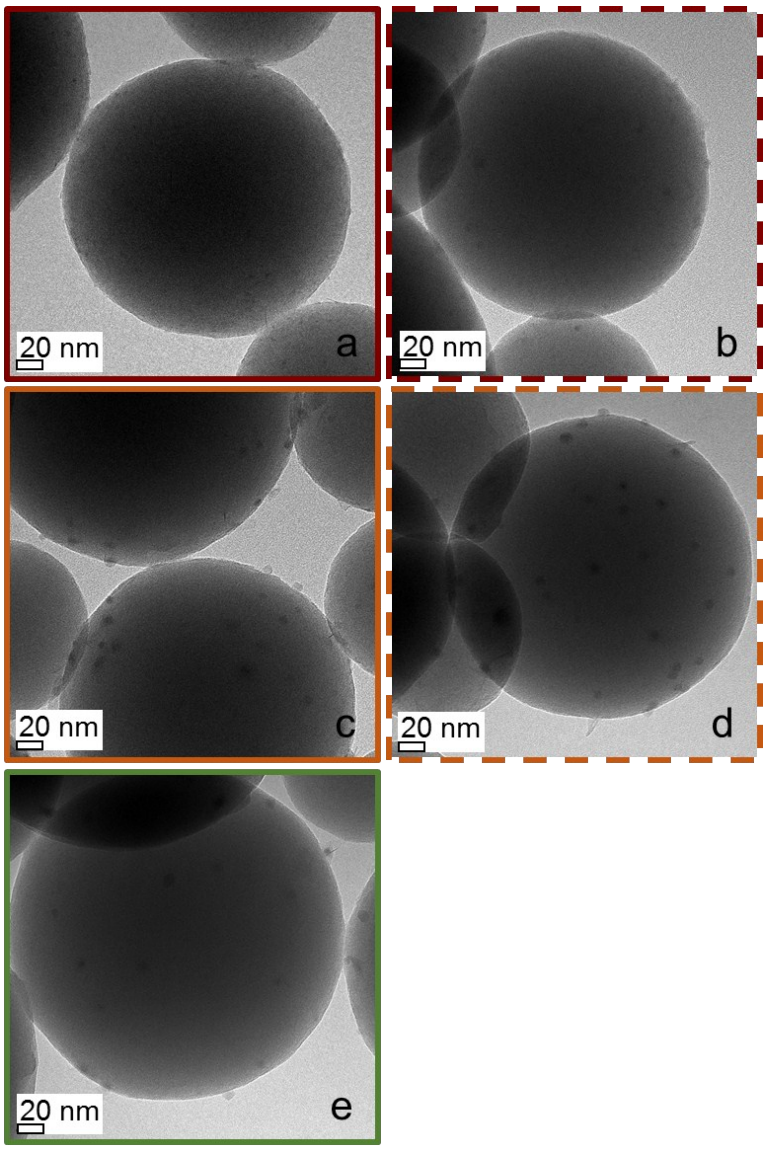

Fig. S11 TEM micrographs of the passivated CAT A after exposure to the distinct H_2O levels in absence of CO (a), CAT A after direct exposure to H_2O level 7 and subsequent Fischer-Tropsch synthesis (b), CAT B after exposure to the distinct H_2O levels in absence of CO (c) and in presence of CO (d), and CAT C after exposure to the distinct H_2O levels in absence of CO (e).

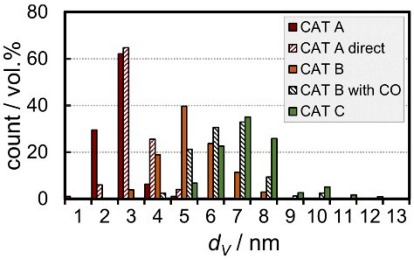

Fig. S12 Volume based size distribution of the crystallites in the passivated samples after exposure to the distinct H_2O levels and re-reduction as obtained via TEM.

Table S1 Physical properties of the model catalysts as obtained from the measurement of the sample magnetisation as a function of external field strength upon reduction.

step	CAT A			CAT A direct			CAT B			CAT B with CO			CAT C		
	M_{rel} / %	γ / %	d_V / nm	M_{rel} / %	γ / %	d_V / nm	M_{rel} / %	γ / %	d_V / nm	M_{rel} / %	γ / %	d_V / nm	M_{rel} / %	γ / %	d_V / nm
reduced	100	0.2	3.2	100	0.1	3.2	100	5.0	5.3	100	4.3	5.3	100	23.7	n/a
dry FT		n/a			n/a			n/a		97.1	5.1	5.4		n/a	
H_2O level 1	105.1	0.1	3.2		n/a		100.7	5.1	5.3	98.5	5.6	5.4	100.6	25.2	n/a
H_2O level 2	104.6	0.3	3.2		n/a		100.9	5.1	5.4	100.3	5.6	5.4	100.4	25.5	n/a
H_2O level 3	99.3	0.4	3.2		n/a		101.7	5.1	5.4	100.9	4.3	5.4	101.2	24.4	n/a
H_2O level 4	84.5	0.3	3.2		n/a		99.5	5.2	5.4	101.4	5.7	5.4	100.7	24.2	n/a
H_2O level 5	78.0	0.9	3.2		n/a		98.3	5.3	5.4	100.2	5.2	5.5	99.3	24.1	n/a
H_2O level 6	70.8	0.5	3.2		n/a		97.3	5.7	5.4	96.0	5.3	5.5	98.8	22.9	n/a
H_2O level 7	56.9	0.8	2.9	55.8	6.4	2.8	96.8	5.5	5.3	92.2	5.7	5.5	98.8	23.5	n/a
H_2O level 7 synthesis gas		n/a		38.4	1.4	2.4		n/a			n/a			n/a	
H_2O level 8	51.1	0.8	2.7		n/a		94.5		n/a	88.8	6.6	5.5	97.0	23.3	n/a
H_2O level 9	23.0	0.5	1.7		n/a			n/a			n/a		74.3	22.1	n/a
dry FT		n/a		46.3	2.0	2.4		n/a			n/a			n/a	
reversibility	31.0	2.5	1.6	50.6	6.6	2.7		n/a		88.7	7.2	5.4	83.9	19.5	n/a
re-reduced	47.2	0.9	1.5	67.3	3.4	2.5		n/a		96.7	8.2	5.5	88.4	21.1	n/a